Interface orbital engineering of large-gap topological states: Decorating gold on a Si(111) surface

Bing Huang,[1,2,*] Kyung-Hwan Jin,[2] Houlong L. Zhuang,[3] Lizhi Zhang,[2] and Feng Liu[2,4,,†]
[1]*Beijing Computational Science Research Center, Beijing 100193, China*
[2]*Department of Materials Science and Engineering, University of Utah, Salt Lake City, Utah 84112, USA*
[3]*Department of Mechanical and Aerospace Engineering, Princeton University, Princeton, New Jersey 08544, USA*
[4]*Collaborative Innovation Center of Quantum Matter, Beijing 100084, China*
(Received 1 November 2015; revised manuscript received 28 January 2016; published 9 March 2016)

Intensive effort has recently been made in search of topological insulators (TIs) that have great potential in spintronics applications. In this paper, a novel concept of overlayer induced interfacial TI phase in conventional semiconductor surface is proposed. The first-principles calculations demonstrate that a p-band-element X (X = In, Bi, and Pb) decorated d-band surface, such as Au/Si(111) surface [X/Au/Si(111)] of an existing experimental system, offers a promising prototype for TIs. Specifically, Bi/Au/Si(111) and Pb/Au/Si(111) are identified to be large-gap TIs. A p-d band inversion mechanism induced by growth of X in the Au/Si(111) surface is revealed to function at different coverage of X with different lattice symmetries, suggesting a general approach of interface orbital engineering of large-gap TIs via tuning the interfacial atomic orbital position of X relative to Au.

DOI: 10.1103/PhysRevB.93.115117

One recent breakthrough in condensed matter physics is topological insulators (TIs) [1,2]. A strong spin-orbital coupling (SOC) interaction associated with nontrivial band inversion can convert a trivial insulating phase into a nontrivial topological insulating phase, in which gapless two-dimensional (2D) surface or one-dimensional (1D) edge states exist inside the bulk band gap of an insulator. A large number of 2D and three-dimensional (3D) TI candidates have been theoretically proposed. To date, several large-gap 3D TIs, e.g., Bi_2Se_3, Bi_2Te_3, and Sb_2Te_3 [3–5], have been experimentally confirmed, while two 2D TIs have been shown experimentally in HgTe/CdTe [6,7] and InAs/GaSb [8] quantum wells, but having too small a gap.

Besides the fact that most theoretically predicted large-gap 2D TIs are metastable, another important reason that makes them difficult for experimental realization is the inevitable substrate effect, which will often alter the intrinsic TI properties [9–12]. In this paper, we investigate an alternative idea to design large-gap interfacial TIs on a semiconductor surface via controlling the orbital alignment between the predesigned overlayer elements and the given surface elements. Our motivation is twofold. First, we focus on experimentally feasible systems based on existing experimental results, especially the well-known growth of heavy metal atoms on semiconductor substrates. Second, we aim at revealing new physical mechanisms to generate TI phases on a surface, which will be generally applicable. To this end, we will illustrate a new concept of "interface orbital engineering" of large-gap TI phases on a substrate through adjusting the atomic orbital coupling between the overalyer atoms and substrate surface atoms.

Growth of metal atoms on Si surfaces has already attracted much interest, e.g., for Rashba spin splitting effect or superconductivity [13–20]. Among the variety of metal-atom induced reconstruction on Si(111) surface, the Au/Si(111) with $\sqrt{3} \times \sqrt{3}$ reconstruction is most well known [17–23]. In this structure, the arrangement of surface Au atoms can be described by the conjugate honeycomb-chained-trimer (CHCT) model [24]. As shown in Fig. 1(a), there is a missing top Si layer on the perfect $(\sqrt{3} \times \sqrt{3})$-Si(111) surface and one additional monolayer of Au atoms sitting on top of the Si surface. The three Au (Si) atoms in the unit cell form a trimer structure.

Both theory and experiment confirm that there is a paraboliclike surface state, mostly contributed by the Au d orbtials, across the Fermi level of Au/Si(111) [Fig. 1(d)] [23,25]. To achieve a possible TI phase in this d-band surface, on top of it we suggest depositing one additional preselected overlayer of p-band-element X. If X has a higher p orbital energy than the Au d orbital energy, a nontrivial p-d band inversion may be realized in the X/Au/Si(111) surface as p and d bands have opposite parity [Fig. 1(e)]. Furthermore, by choosing X, a sizable SOC gap can be opened at the p-d crossing (Dirac) point [Fig. 1(f)], hence a 2D TI phase can be created. We point out that our design principle is mechanistically different from the previously reported orbital filtering effect for the realization of 2D TI on the semiconductor surface [26,27], although both involve metal-decorated semiconductor surfaces. Most notably, the previous approach works only for a fixed coverage of metal overlayer with hexagonal lattice, while our new approach is applicable to different coverage and lattice symmetries, e.g., hexagonal and trigonal. Below, we will use first-principles calculations to demonstrate our design principles (see computational details in Ref. [25]).

The Au/Si(111) surface has been experimentally shown to be a suitable template for epitaxial growth of metal-atom overlayers. For example, Na, Cs, In, and Tl monolayer structures have been grown on Au/Si(111) surface with different domain sizes [21–23]. Based on our design principle [Fig. 1(d)], we first consider In and Tl as the overlayer element X, because their p orbital energies are higher than the Au d orbital energy (-2.78 eV for In $5p$, -2.66 eV for Tl $6p$, and -7.14 eV for Au $5d$). On Au/Si(111) surface, there are three nonequivalent high-symmetry adsorption sites for metal atom X, as shown in Fig. 1(a). Site I (II) represents the hollow site of Si (Au) trimer, while site III represents the top site of Si atom between two

*Bing.Huang@csrc.ac.cn
†fliu@eng.utah.edu

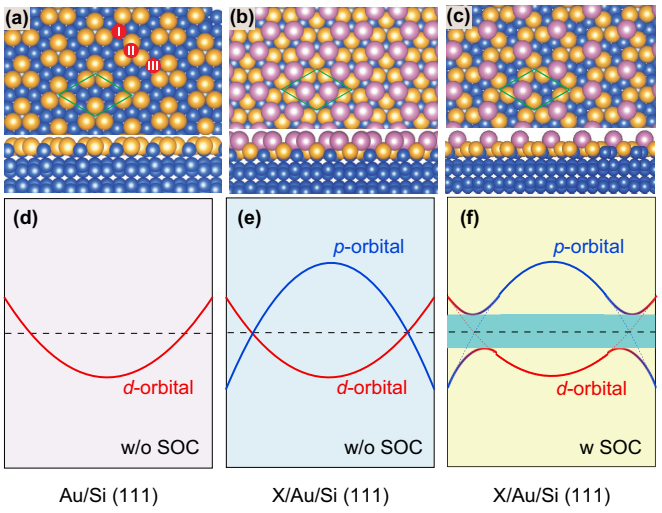

FIG. 1. (a) The CHCT structure model of Au/Si(111) surface with $\sqrt{3} \times \sqrt{3}$ reconstruction. The sites I, II, and III represent three nonequivalent high-symmetry adsorption sites for metal-atom X adsorption. (b) and (c) are the X/Au/Si(111) surface structure models with $\frac{2}{3}$ ML and $\frac{1}{3}$ ML X atoms, respectively. Both the top view (upper) and side view (lower) are shown in (a)–(c). The unit cell in (a)–(c) is marked by green solid lines, and the blue, golden, and pink colors represent Si, Au, and X, respectively. (d)–(f) Schematic illustration of the overlayer induced band inversion in X/Au/Si(111). (d) The existence of a paraboliclike Au d-band surface state across the Fermi level (without SOC). (e) The p-band-element X overlayer induces a p-d band inversion (without SOC). (f) A sufficiently large SOC opens a sizable band gap around the Dirac point to realize a TI phase.

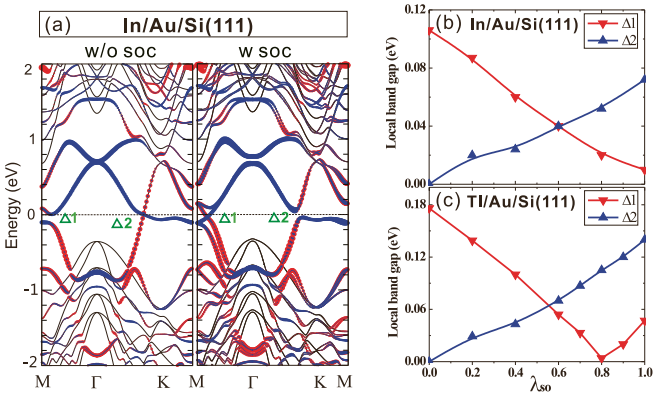

FIG. 2. (a) The electronic band structures of $\frac{2}{3}$ ML In/Au/Si(111) without and with SOC. The red and blue dots represent the distribution of Au d and In p orbitals, respectively. The sizes of red/blue dots reflect the weight of the corresponding d/p states. The Fermi level is set to zero. The gap sizes of $\triangle 1$ and $\triangle 2$ as a function of λ_{so} for $\frac{2}{3}$ ML In/Au/Si(111) and $\frac{2}{3}$ ML Tl/Au/Si(111) are shown in (b) and (c), respectively.

Au trimers. Our calculations show that the adsorption energy of In (Tl) at site I is 0.39 (0.37) and 0.38 (0.35) eV lower than that of site II and site III, respectively. There is no surprise that the stability of In and Tl on Au/Si(111) is almost the same, as In and Tl have the same number of valence electron/atomic size. If we assume the site I on the surface can be fully (half) occupied, then $\frac{2}{3}$ ML ($\frac{1}{3}$ ML) coverage of In/Tl atoms can form a hexagonal (triangular) lattice, as shown in Fig. 1(b) [Fig. 1(c)]. Indeed, the hexagonal-like In and Tl lattices on Au/Si(111) surface have been observed in scanning tunneling microscopy measurements [21–23].

Let us now examine the electronic structure of $\frac{2}{3}$ ML X on Au/Si(111) [Fig. 1(b)] with hexagonal X lattice. The calculated band structure of In/Au/Si(111) without SOC is shown in Fig. 2(a) (left panel). As seen from the projected band structure, the bands around Fermi level are mostly contributed by the Au d orbitals and In p orbitals. The crossing between the p and d states gives rise to a Dirac point (marked as $\triangle 2$) at the Fermi level along the Γ-K line of the Brillouin zone. The atomic orbital alignment between In $5p$ and Au $5d$ gives rise to a p-d band inversion across the Fermi level, consistent with our design principle [Fig. 1(e)] and suggesting a possible nontrivial band topology [7]. Furthermore, the p-d coupling opens a local anticrossing band gap of 0.11 eV around the M point (marked $\triangle 1$), which is called interface hybridization charge (IHC) gap since it is induced by charge localization associated with interface orbital hybridization. When SOC effect is considered, SOC lifts the degeneracy of Dirac point and opens a local SOC gap of 0.07 eV at $\triangle 2$ [Fig. 2(a), right panel]. Meanwhile, the surface Rashba effect splits the band degeneracy in the presence of SOC, which can be more clearly seen along the M-Γ line of the Brillouin zone [Fig. 2(a), right panel]. Specifically, the band splitting of the bottom conduction band and top valence band along the M-Γ line significantly reduces the IHC gap at $\triangle 1$ to 0.01 eV.

To better understand the SOC effect, we have artificially increased the strength of SOC (λ_{so}) from 0 to its full value 1 in the calculation and monitor the evolution of band structure. As shown in Fig. 2(b), when λ_{so} is increased, the IHC gap at $\triangle 1$ decreases monotonically, while the SOC gap at $\triangle 2$ increases monotonically. Finally, the local conduction band minimum at $\triangle 1$ and the local valence band maximum at $\triangle 2$ almost merge, resulting in a $\sim$5 meV global band gap (enlarged to 36 meV under HSE calculations). Moreover, the calculated topological Z_2 invariant is 1 in In/Au/Si(111), confirming its nontrivial TI phase.

The electronic structure of $\frac{2}{3}$ ML Tl/Au/Si(111) is almost the same as that of In/Au/Si(111) [25]. However, a significant difference has been found when we evaluate the evolution of $\triangle 1$ vs $\triangle 2$ as a function of λ_{so}. As shown in Fig. 2(c), $\triangle 1$ monotonously decreases when $0 < \lambda_{so} < 0.8$, but it closes at $\lambda_{so} = 0.8$ and reopens again for $\lambda_{so} > 0.8$. This additional band inversion around the M point happens to convert Tl/Au/Si(111) from a TI to a trivial insulator. An even (odd) number of band inversions indicates a trivial (nontrivial) insulator. The calculated Z_2 invariant is confirmed to be 0 [25].

The above study shows that although there exists a nontrivial p-d band inversion across the Fermi level, the surface Rashba effect can close or even reopen the original small IHC gap $\triangle 1$ and eventually results in either a tiny nontrivial TI gap in In/Au/Si(111) or an even trivial gap in Tl/Au/Si(111). In order to realize a large-gap TI phase in X/Au/Si(111), a sufficient large $\triangle 1$ gap is desired by carefully selecting new p-band-element X. As the size of $\triangle 1$ is mostly determined by

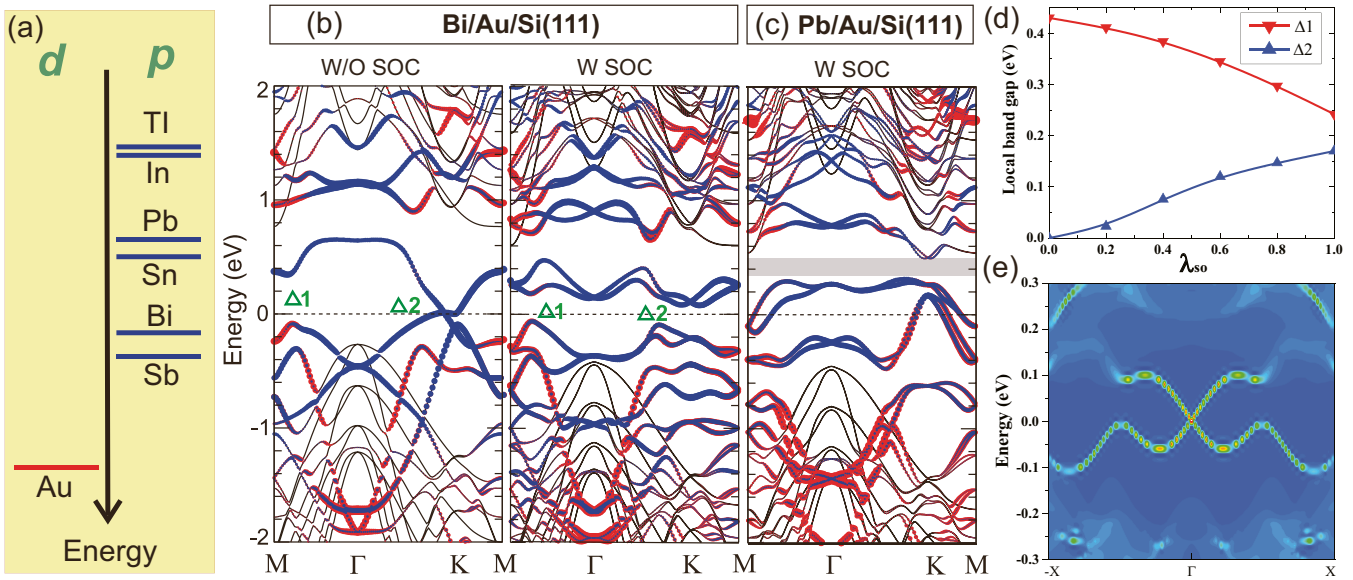

FIG. 3. (a) The diagram of energy level alignment between the atomic Au d orbital and atomic X p orbitals (X = Tl, In, Pb, Sn, Bi, Sb). (b) The electronic band structure of Bi/Au/Si(111) without and with SOC. (c) The electronic band structure of Pb/Au/Si(111) with SOC. The line labels are the same as Fig. 2. (d) The gap size of $\triangle 1$ and $\triangle 2$ in Bi/Au/Si(111) as a function of λ_{so}. (e) The energy and momentum-dependent local density of state of the zigzag edge of semi-infinite Bi/Au/Si(111).

the interfacial p-d coupling strength, a suitable X must have a much stronger p_X-d_{Au} coupling strength than that of In/Tl. Ideally, the strength of p_X-d_{Au} coupling largely depends on the energy level proximity between Au d orbitals and X p orbitals, i.e., the closer these two energy levels are, the stronger the p-d coupling will be. Also, since the deposition of In/Tl atoms on Au/Si(111) has been proved experimentally, we focus on new X candidates having similar valence p electrons and atomic sizes as In and Tl, in order to have similar stability. Thus, we have examined Pd, Sn, Bi and Sb atoms. As shown in Fig. 3(a), compared to the energy levels of In $5p$ (-2.78 eV) and Tl $6p$ (-2.66 eV), the Pd $6p$ (-3.79 eV), Sn $5p$(-3.96 eV), Bi $6p$ (-4.86 eV), and Sb $5p$ (-5.08 eV) levels are closer to the energy level of the Au $5d$ orbital ($-7.14eV$). The selected X candidates also have a close number of electrons compared to In/Tl. Moreover, the atomic sizes of Pb, Sn, Bi, and Sb are all similar to those of In and Tl.

We have calculated the adsorption energies of these X candidates on Au/Si(111) surface, and indeed they are (at least) as stable as that of In and Tl on Au/Si(111) surface. The adsorption energy of a Bi (Pb) atom at site I is 0.64 and 0.57 (0.77 and 0.85) eV lower than that at site II and site III, respectively. It is therefore reasonable to expect that Bi and Pb might also been grown on Au/Si(111) surface as In/Au/Si(111). The stability of Sn/Sb on Au/Si(111) surface is also similar to that of the Pb/Bi cases (not shown here).

For the $\frac{2}{3}$ ML Bi/Au/Si(111) system, as shown in Fig. 3(b), the size of IHC gap $\triangle 1$ is remarkably increased to 0.43 eV (without SOC), which is more than twice larger than that in the In and Tl systems (<0.2 eV), consistent with our initial reasoning. As λ_{so} increases, the size of $\triangle 1$ is gradually decreased to 0.24 eV, and meanwhile the SOC gap $\triangle 2$ is gradually increased to 0.18 eV [Fig. 3(d)]. The global band gap for this system is 0.15 (0.28) eV under Perdew-Burke-Ernzerhof (PBE) [Heyd-Scuseria-Ernzerhof (HSE)] calculations. The calculated Z_2 invariant is 1 in Bi/Au/Si(111), confirming its nontrivial TI phase [25]. As another hallmark of 2D TI is the existence of gapless helical edge states inside the bulk band gap, we have also calculated the topological edge states by constructing the edge Green's function of a semi-infinite Bi/Au/Si(111) surface. The local density of states of the zigzag edge is shown in Fig. 3(e), which shows that the gapless edge states, connecting the upper and lower bulk band edges and forming a 1D Dirac cone at the Brillouin zone boundary, are characterized by an odd number of crossings over the Fermi level, indicative of their topological protection. We note that the mechanism for creating TI phase in the Bi/Au/Si(111) system is totally different from the previously reported orbital filtering mechanism in the Bi/Cl/Si(111) system [26].

The situation of $\frac{2}{3}$ ML Pb/Au/Si(111) is similar to that of Bi/Au/Si(111), except that it is a p-type-like TI system, as shown in Fig. 3(c). The strong p-d coupling strength gives rise to a sufficiently large TI gap of 0.18 (0.39) eV [shadow zone in Fig. 3(c)] above Fermi level under PBE (HSE) calculations [25]. The calculated Z_2 invariant is 1 when the Fermi level is artificially moved into the SOC gap. In practice, the Fermi level of Si substrate can be readily tuned by gating with standard techniques. For the cases of $\frac{2}{3}$ ML Sn/Au/Si(111) and $\frac{2}{3}$ ML Sb/Au/Si(111), although the size of IHC gap $\triangle 1$ can be enhanced according to our design principle, the lack of a global TI gap in these systems makes them less interesting and are not discussed here.

Next, we demonstrate that overlayer X induced nontrivial p-d band inversion in the X/Au/Si(111) system can also exist at a lower X coverage, e.g., $\frac{1}{3}$ ML X with trigonal symmetry [Fig. 1(c)]. This could be practically even more important because it may be difficult for experiment to choose one coverage [21,23]. Our calculations show that although all the

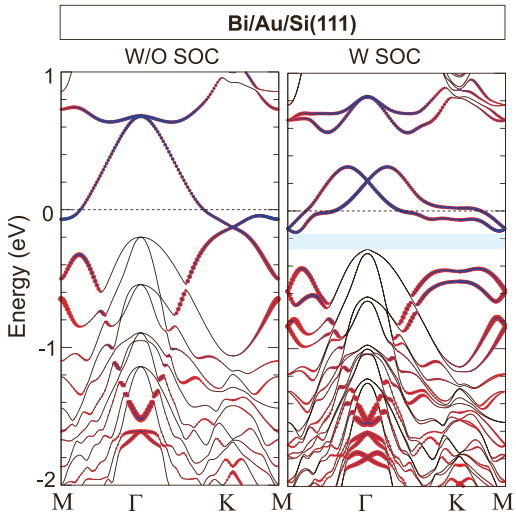

FIG. 4. The electronic band structure of $\frac{1}{3}$ ML Bi/Au/Si(111) without and with SOC. The line labels are the same as Fig. 2.

$\frac{1}{3}$ ML In, Tl, Bi, and Pb overlayers can induce a p-d band inversion, only Bi and Pb overlayer induced band inversions are topologically nontrivial ($Z_2 = 1$). As shown in Fig. 4, $\frac{1}{3}$ ML Bi/Au/Si(111) surface has a p-d band crossing (Dirac) point at ~0.1 eV below the Fermi level and the SOC effect can lift this degeneracy and induce a global 0.13 (0.25) eV gap from PBE (HSE) calculations. Similarly, the $\frac{1}{3}$ ML Pb/Au/Si(111) system can also host an intrinsic 0.02 (0.05) eV gap around the Fermi level [25]. Also, it is not straightforward to directly compare the band structures of $\frac{2}{3}$ ML and $\frac{1}{3}$ ML Bi/Au/Si(111) in detail, as they have a different number of Bi atoms (i.e., electronic bands) and different lattice symmetry. But we can clearly see the band inversion between the Bi and Au states in both band structures, which is the key for the realization of TI phase. Therefore, these calculations demonstrate that the p-band-element overlayer induced nontrivial p-d inversion on d-band Au/Si(111) in general may occur at different coverage of X in different lattice symmetries, significantly easing the way for experimental realization.

TABLE I. The topological invariant Z_2 and band gap E_g of X/Au/Si(111) (X = In, Tl, Bi, and Pb) at $\frac{1}{3}$ ML and $\frac{2}{3}$ ML X coverage. The HSE band gap is listed in parentheses. It is noted that $\frac{2}{3}$ ML Pb/Au/Si(111) and $\frac{1}{3}$ ML In/Au/Si(111) are p-type semiconductors, while $\frac{1}{3}$ ML Bi/Au/Si(111) is n type.

$\frac{2}{3}$ ML	Z_2	E_g (eV)	$\frac{1}{3}$ ML	Z_2	E_g (eV)
In	1	0.005 (0.036)	In	0	0.052 (0.112)
Tl	0	0.047 (0.068)	Tl	0	0 (0)
Bi	1	0.146 (0.276)	Bi	1	0.125 (0.254)
Pb	1	0.182 (0.391)	Pb	1	0.022 (0.046)

In summary, we have systemically investigated the mechanism of p-band-metal overlayer induced TI phase in d-band Au/Si(111) surface (Table I). Broadly, our findings may be extended to the search for new 2D TI materials including magnetic TI phases for quantum anomalous Hall effect on other conventional semiconductor surfaces with overlayer induced nontrivial band inversion.

The research at Utah was supported by US Department of Energy (Grant No. DE-FG02-04ER46148). B.H. acknowledges the support from Chinese Youth 1000 Talents Program and NSFC (Grant No. 1157041396). Computations were performed at DOE-NERSC and CHPC of University of Utah.

[1] M. Z. Hasan and C. L. Kane, Rev. Mod. Phys. **82**, 3045 (2010).
[2] X.-L. Qi and S.-C. Zhang, Rev. Mod. Phys. **83**, 1057 (2011).
[3] H. Zhang, C. Liu, X. L. Qi, X. Dai, Z. Fang, and S.-C. Zhang, Nat. Phys. **5**, 438 (2009).
[4] Y. L. Chen, J. G. Analytis, J.-H. Chu *et al.*, Science **325**, 178 (2009).
[5] Y. Xia, D. Qian, D. Hsieh *et al.*, Nat. Phys. **5**, 398 (2009).
[6] B. A. Bernevig, T. L. Hughes, and S. C. Zhang, Science **314**, 1757 (2006).
[7] M. König, S. Wiedmann, C. Brüne, A. Roth, H. Buhmann, L. W. Molenkamp, X.-L. Qi, and S.-C. Zhang, Science **318**, 766 (2007).
[8] I. Knez, R.-R. Du, and G. Sullivan, Phys. Rev. Lett. **107**, 136603 (2011).
[9] F. Yang, L. Miao, Z. F. Wang, M. Yao, F. Zhu, Y. R. Song, M. Wang, J. Xu, A. V. Fedorov, Z. Sun, G. B. Zhang, C. Liu, F. Liu, D. Qian, C. L. Gao, and J. Jia, Phys. Rev. Lett. **109**, 016801 (2012).
[10] T. Hirahara, N. Fukui, T. Shirasawa, M. Yamada, M. Aitani, H. Miyazaki, M. Matsunami, S. Kimura, T. Takahashi, S. Hasegawa, and K. Kobayashi, Phys. Rev. Lett. **109**, 227401 (2012).
[11] L. Miao, Z. F. Wang, W. Ming, M. Yao, M. Wang, F. Yang, Y. R. Song, F. Zhu, A. V. Fedorov, Z. Sun, C. L. Gao, C. Liu, Q. Xuee, C. Liu, F. Liu, and J. Jia, Proc. Natl. Acad. Sci. USA **110**, 2758 (2013).
[12] F. Zhu, W. Chen,Y. Xu, C. Gao, D. Guan, C. Liu, D. Qian, S. Zhang, and J. Jia, Nat. Mater. **14**, 1020 (2015).
[13] I. Gierz, T. Suzuki, E. Frantzeskakis, S. Pons, S. Ostanin, A. Ernst, J. Henk, M. Grioni, K. Kern, and C. R. Ast, Phys. Rev. Lett. **103**, 046803 (2009).
[14] K. Sakamoto, H. Kakuta, K. Sugawara, K. Miyamoto, A. Kimura, T. Kuzumaki, N. Ueno, E. Annese, J. Fujii, A. Kodama, T. Shishidou, H. Namatame, M. Taniguchi, T. Sato, T. Takahashi, and T. Oguchi, Phys. Rev. Lett. **103**, 156801 (2009).
[15] K. Sakamoto, T. Oda, A. Kimura, K. Miyamoto, M. Tsujikawa, A. Imai, N. Ueno, H. Namatame, M. Taniguchi, P. E. J. Eriksson, and R. I. G. Uhrberg, Phys. Rev. Lett. **102**, 096805 (2009).
[16] J. Park, S. W. Jung, M. C. Jung, H. Yamane, N. Kosugi, and H. W. Yeom, Phys. Rev. Lett. **110**, 036801 (2013).
[17] H. R. Bishop and J. C. Riviere, J. Phys. D **2**, 1635 (1969).
[18] T. Nagao, S. Hasegawa, K. Tsuchie, S. Ino, C. Voges, G. Klos, H. Pfnür, and M. Henzler, Phys. Rev. B **57**, 10100 (1998).
[19] E. A. Khramtsova and A. Ichimiya, Phys. Rev. B **57**, 10049 (1998).

[20] H. M. Zhang, T. Balasubramanian, and R. I. G. Uhrberg, Phys. Rev. B **65**, 035314 (2001).

[21] D. V. Gruznev, I. N. Filippov, D. A. Olyanich, D. N. Chubenko, I. A. Kuyanov, A. A. Saranin, A. V. Zotov, and V. G. Lifshits, Phys. Rev. B **73**, 115335 (2006).

[22] J. K. Kim, K. S. Kim, J. L. McChesney, E. Rotenberg, H. N. Hwang, C. C. Hwang, and H. W. Yeom, Phys. Rev. B **80**, 075312 (2009).

[23] L. V. Bondarenko, D. V. Gruznev, A. A. Yakovlev, A. Y. Tupchaya, D. Usachov, O. Vilkov, A. Fedorov, D. V. Vyalikh, S. V. Eremeev, E. V. Chulkov, A. V. Zotov, and A. A. Saranin, Sci. Rep. **3**, 1826 (2013).

[24] Y. G. Ding, C. T. Chan, and K. M. Ho, Surf. Sci. **275**, L691 (1992).

[25] See Supplemental Material at http://link.aps.org/supplemental/10.1103/PhysRevB.93.115117 for the details of computational methods, electronic structure of X/Au/Si(111), topological Z_2 invariant calculations, and the HSE band structures of X/Au/Si(111).

[26] M. Zhou, W. Ming, Z. Liu, Z. Wang, P. Li, and F. Liu, Proc. Natl. Acad. Sci. USA **111**, 14378 (2014).

[27] C. Hsu, Z. Huang, F. Chuang, C. Kuo, Y.-T. Liu, H. Lin, and A. Bansil, New J. Phys. **17**, 025005 (2015).